ELSEVIER

International Journal of Heat and Fluid Flow 20 (1999) 385–394

International Journal of HEAT AND FLUID FLOW

www.elsevier.com/locate/ijhff

On the development of a computational method for modelling turbulent mixing in sharply stratified flows

A.G. Straatman [1]

Department of Mechanical and Materials Engineering, University of Western Ontario, London, Ont., Canada N6A 5B9

Received 11 March 1998; accepted 2 December 1998

Abstract

A method is presented for computationally modelling turbulent mixing across a sharp stable interface. The turbulence is modelled using a second-moment stress/flux closure because of the anisotropy due to stratification, and the additional anisotropy due to the presence of the sharp interface. The numerical method utilizes an adaptive, moving-grid formulation of the governing transport equations, and solves for the movement of the interface implicitly with the solution of the transport equations. The implicit prediction of the interfacial movement is based on a special solution of the discrete scalar equation for the upper-most control-volume, which is assumed to reside partly in the non-active layer above the interface. Results are presented for the case of mixing due to oscillating-grid turbulence and compared to experimental data. The present predictions demonstrate the viability of the computational method, and the validity of the second-moment closure in sharply stratified flows.

Keywords: Stable stratification; Finite-volume technique; Second-moment turbulence closure

Notation

A	area of control-volume face
$\mathscr{A}_\epsilon$	coefficient in $\epsilon = \mathscr{A}_\epsilon u_{1o}^3/l_o$
B_1, B_2	constants in spatial decay expressions
C	coefficients in modelled turbulence equations
$\mathscr{D}$	diffusion term in transport equation
D_a	initial depth of active layer
D_n, D_s	diffusion coefficients in discrete transport equations
f	function in wall-reflection models
D_t	total depth of active layer
E	dimensionless entrainment, u_e/u_{1o}
g_i	gravity vector
$\mathscr{G}$	buoyancy production in transport equation
h	movement of interface
jb, je	beginning and ending indices of grid
k	turbulent kinetic energy
l	integral length scale of turbulence
L_P	coefficient in Lumley diffusion model
$\dot{m}$	mass flux through control-volume face
M_P	mass of control-volume centered at P
n	exponent in entrainment law
n_i	unit normal vector
$\overline{p'u_k}$	pressure–velocity correlation
$\mathscr{P}$	production term in transport equation
R	scale factor for dissipation of scalar intensity
Re_l	Reynolds number based on integral length scale
Re_λ	Reynolds number based on Taylor microscale
Ri	local Richardson number
$\mathscr{S}$	surface area
t	time
$\mathscr{T}_{ijk}$	component in Lumley diffusion model
$\overline{u_iu_j}$	Reynolds-stresses (per ρ)
$\overline{u_iu_ju_k}$	turbulent transport in Reynolds-stress equation
$\overline{u_k\phi}$	scalar-fluxes (per ρ)
$\overline{u_i}$	RMS fluctuating velocities (eg. $\overline{u_1} = (\overline{u_1u_1})^{1/2}$)
u_{io}	RMS fluctuating velocity in non-stratified oscillating-grid turbulence
u_e	entrainment velocity
$\mathscr{U}_i$	velocity
$\overline{U}_i$	mean fluid velocity
U_g	grid velocity
$\mathscr{V}$	volume
x_i	Cartesian coordinates
x_n	normal distance from interface

Greek

α	weighting factor in advection scheme
β	volumetric expansion coefficient
Γ^ϕ	molecular diffusivity of Φ
δ_{ij}	Kronecker delta
ϵ	dissipation term in transport equation
ϵ	isotropic dissipation rate of k
κ	von Karman coefficient
λ	Taylor microscale of turbulence

[1] Tel.: +1-519-679-2111; fax: +1-519-661-3020; e-mail: astraat@ngga.uwo.ca

0142-727X/99/$ – see front matter
PII: S0142-727X(98)10059-0

ξ distance from interface
π pressure–strain term in transport equation
ρ fluid density
$\overline{\Phi}$ general mean scalar
$\overline{\phi\phi}$ scalar intensity

Superscripts and subscripts
n,s north and south faces of control-volume
N, P, S nodal points
o (super) value at previous time-step
o (sub) indicates value in non-stratified oscillating-grid turbulence
∞ level of non-active layer

1. Introduction

Stable stratification and sharp density interfaces exist in many geophysical, environmental and industrial flows. Some well-known examples are the abrupt interfaces that exist between fresh and salinated waters in the ocean, the top of the atmospheric boundary layer, and heavier-than-air gas flows. The prediction of such flows is useful for studying the evolution of various flow systems, but more importantly, for determining the rate of dispersion of heavier-than-air pollutants into the atmosphere.

Sharply stratified flows are characterized by an *active* layer in which turbulence is produced or maintained, a sharp interface, and a relatively uniform *non-active* layer. Because of the sharp stratification, relatively little shear occurs at the interface and thus, turbulence that exists in the active layer is primarily produced by ground-shear. The turbulence in the vicinity of the interface is acutely attenuated to the extent that the interface appears as a barrier between the active and non-active layers. Entrainment of fluid across the interface, and thus the dispersion of the active layer, is due to ground-produced turbulence being transported into the interface by diffusive transport. We note that while turbulence can exist in both the active and non-active layers, the scales are typically quite different – consider, for example a heavier-than-air gas flow – and it is the turbulence in the active layer that drives the entrainment process.

On the basis of this description, the accuracy of computational predictions in sharply stratified flows is expected to depend mainly on the treatment of turbulence in the vicinity of the interface, and on the modelling of diffusive transport. To properly account for these effects, plus the additional effects of stratification, a second-moment turbulence closure was incorporated in the present work. In a second-moment closure, the effects of stratification are accounted for naturally in the formulation, and the issue of diffusion can be addressed through the selection of an appropriate model. The selection of a model for the diffusion of the turbulent stresses is based on the model performance in isothermal flows since diffusion is only weakly influenced by thermal gradients. An additional model can also be implemented to account for the extra attenuation of turbulence in the region of the interface. However, to properly model the attenuation of turbulence at the interface, the position of the interface must be known. Thus, a principal element of this study was the development of a computational method which predicts the position of the interface.

The method which was developed predicts the movement of the sharp interface implicitly with the solution of the governing field equations. By *tracking* the interface in this manner, the present method addresses the issue of locating the interface, but also has other advantages. First, it is only *necessary* to model the active layer since the non-active layer does not have an influence on the entrainment process. Second, the present method circumvents common numerical difficulties associated with the movement of a sharp interface across a fixed grid by allowing the computational grid to move, or adapt, with the movement of the interface.

The purpose of this paper is to demonstrate that the present computational method, used in the framework of a second-moment turbulence closure, gives reasonable predictions of entrainment through a stably stratified interface. Because the physical effects which influence entrainment do not directly involve the mean flow field, the computational model is described and validated herein for a one-dimensional case. Working in a one-dimensional framework significantly reduces the details to be presented while retaining the important physical effects which form the basis of the method. Furthermore, the one-dimensional predictions can be directly validated with data from oscillating-grid experiments. Experiments using oscillating-grid turbulence have been carried out in the past to examine the entrainment across sharp density interfaces (Thompson and Turner, 1975; Hopfinger and Toly, 1976; Fernando and Long, 1985; E and Hopfinger, 1986; Nokes, 1988; De Silva and Fernando, 1994, 1996), the movement of turbulence fronts (Dickinson and Long, 1978, 1983), and the structure of turbulence in the vicinity of a sharp density interface (Hannoun et al., 1988).

This paper is presented in three main sections. In Section 2, the mathematical formulation is presented, including modelled equations for all independent variables and the method used to model the attenuation of turbulence in the vicinity of the interface. Section 3 describes the discretization technique and the method developed for computing the movement of the interface. Section 4 contains systematic comparisons between results computed using the present method and data from oscillating-grid turbulence experiments.

2. Transport equations

The transport equations and turbulence model equations presented in this section are only those required for the prediction of stably stratified oscillating-grid turbulence. As described in Section 1, this one-dimensional case isolates the important effects of the entrainment process and thereby allows us to validate the physical basis of the present method in a much simpler framework. For this one-dimensional case, no mean flow exists and it is, therefore, not necessary to solve the conservation equations for mass and momentum.

Where modelling was required in the transport equations, a near-standard approach has been taken. This approach was taken mainly to avoid obfuscating the present computational model with several complicated closure approximations. The only departures from the standard models are in the modelling of the diffusion of the Reynolds stresses (for reasons forthcoming) and in the treatment of the inhibiting effect of the interface on the turbulence.

2.1. Mean scalar transport

Scalar variations are described by the following time-averaged equation for the transport of a general scalar Φ:

$$\frac{\partial \rho \overline{\Phi}}{\partial t} + (\rho \overline{U}_k \, \overline{\Phi})_{,k} = (\rho \Gamma^{\Phi} \overline{\Phi}_{,k})_{,k} - (\rho \overline{u_k \phi})_{,k}, \tag{1}$$

where the last term on the right-hand side of Eq. (1) represents the net influence of turbulence on the scalar transport. This so-called *scalar-flux* term, in general, represents three additional unknowns for which a model must be provided. In the present case, however, only one scalar-flux component is non-zero.

2.2. Reynolds-stress transport equation

The Reynolds-stresses are obtained from the following transport equation:

$$\frac{\partial \rho \overline{u_i u_j}}{\partial t} + (\rho \overline{U}_k \ \overline{u_i u_j})_{,k} = \rho(\mathscr{D}_{ij} + \mathscr{P}_{ij} + \mathscr{G}_{ij} + \pi_{ij} - \epsilon_{ij}). \tag{2}$$

The terms on the right-hand side of Eq. (2) represent the diffusive transport, the shear production, the buoyancy production, the pressure-redistribution, and the dissipation of $\overline{u_i u_j}$. To obtain a closed mathematical framework, some of these processes must be modelled in terms of other dependent variables. The shear production and buoyancy production do not require modelling and are given as:

$$\mathscr{P}_{ij} = -(\overline{u_i u_k} \ \overline{U}_{j,k} + \overline{u_j u_k} \ \overline{U}_{i,k}), \tag{3}$$

$$\mathscr{G}_{ij} = -\beta(g_i \ \overline{u_j \phi} + g_j \ \overline{u_i \phi}). \tag{4}$$

Standard relations given by, for example, Launder (1989) were used to model the pressure-redistribution and dissipation terms. Regarding the pressure-redistribution term, the common practice is to recast π_{ij} as the sum of three components:

$$\pi_{ij} = \pi_{ij,1} + \pi_{ij,2} + \pi_{ij,3} \tag{5}$$

which represent respectively the pressure interaction with turbulent motions, the pressure interaction with mean strain and the pressure interaction with buoyancy. Standard models for the three components are given as:

$$\pi_{ij,1} = -C_1 \frac{\epsilon}{k}\left(\overline{u_i u_j} - \frac{2}{3} k \delta_{ij}\right), \tag{6}$$

$$\pi_{ij,2} = -C_2\left(\mathscr{P}_{ij} - \frac{1}{3}\mathscr{P}_{kk}\delta_{ij}\right), \tag{7}$$

$$\pi_{ij,3} = -C_3\left(\mathscr{G}_{ij} - \frac{1}{3}\mathscr{G}_{kk}\delta_{ij}\right), \tag{8}$$

where $k = \overline{u_k u_k}/2$ is the turbulent kinetic energy and ϵ the isotropic dissipation rate of k. The dissipation of $\overline{u_i u_j}$ is assumed isotropic and is modelled as:

$$\epsilon_{ij} = \frac{2}{3}\epsilon \delta_{ij}. \tag{9}$$

Because of the importance of diffusive transport in sharply stratified flows, the diffusion of $\overline{u_i u_j}$ was not approximated using a standard closure model. Typically, diffusion is regarded as being unimportant in the Reynolds-stress budget, and is modelled using the Daly and Harlow (1970) relation. While the Daly and Harlow (1970) model is relatively simple to implement, it is widely known that the model is not physically nor mathematically correct. In this study, the Lumley (1978) model was used with the modification suggested by Straatman et al. (1998). Straatman et al. (1998) showed that the Lumley (1978) model is the only existing diffusion model which contains components that can account for all of the important processes in $\mathscr{D}_{ij}$. The Lumley (1978) model is most easily described starting from the exact form of the diffusion process (neglecting viscous diffusion):

$$\mathscr{D}_{ij} = -\left(\overline{u_i u_j u_k} + \frac{\overline{p' u_i}}{\rho}\delta_{kj} + \frac{\overline{p' u_j}}{\rho}\delta_{ki}\right)_{,k}. \tag{10}$$

The components are then modelled as:

$$-\overline{u_i u_j u_k} = C_{s1}\frac{k}{\epsilon}\left(\mathscr{T}_{ijk} + C_{s2}\left(\mathscr{T}_i \ \delta_{jk} + \mathscr{T}_j \ \delta_{ik} + \mathscr{T}_k \ \delta_{ij}\right)\right),$$

$$\frac{1}{\rho}\overline{p' u_k} = -\frac{1}{5} \ L_P \ \overline{u_k u_m u_m},$$

where:

$$\mathscr{T}_{ijk} = \overline{u_i u_l} \ (\overline{u_j u_k})_{,l} + \overline{u_j u_l} \ (\overline{u_i u_k})_{,l} + \overline{u_k u_l} \ (\overline{u_i u_j})_{,l}$$

and $\mathscr{T}_i = \mathscr{T}_{imm}$.

The coefficients in the model relations for the Reynolds-stress equation are summarized as:

$$\{C_s, C_{s2}, L_P, C_1, C_2, C_3\} = \{0.098, 0.128, 0.80, 1.80, 0.60, 0.30\}. \tag{11}$$

2.3. Scalar-flux transport equation

The scalar-fluxes are obtained from the following transport equation:

$$\frac{\partial \rho \overline{u_i \phi}}{\partial t} + (\rho \overline{U}_k \ \overline{u_i \phi})_{,k} = \rho(\mathscr{D}_{i\phi} + \mathscr{P}_{i\phi} + \mathscr{G}_{i\phi} + \pi_{i\phi} - \epsilon_{i\phi}). \tag{12}$$

The terms on the right-hand side represent the diffusion, the production due to mean shear and mean scalar gradients, the buoyancy production, the pressure-interaction, and the dissipation of $\overline{u_i \phi}$. As in the Reynolds-stress equation, the production terms require no approximation and their exact forms are given as:

$$\mathscr{P}_{i\phi} = -(\overline{u_k \phi} \ \overline{U}_{i,k} + \overline{u_i u_k} \ \overline{\Phi}_{,k}), \tag{13}$$

$$\mathscr{G}_{i\phi} = -g_i \beta \overline{\phi\phi}. \tag{14}$$

The pressure-interaction term is subdivided into three components:

$$\pi_{i\phi} = \pi_{i\phi,1} + \pi_{i\phi,2} + \pi_{i\phi,3}, \tag{15}$$

which are associated respectively with purely turbulent motions, with mean strain and mean scalar gradients, and with buoyancy forces. Models for each of these components were taken from Rodi (1982) and are given as:

$$\pi_{i\phi,1} = -C_{1\phi}\frac{\epsilon}{k} \ \overline{u_i \phi}, \tag{16}$$

$$\pi_{i\phi,2} = C_{2,\phi}\overline{u_i \phi} \ \overline{U}_{i,k}, \tag{17}$$

$$\pi_{i\phi,3} = -C_{3\phi} g_i \beta \ \overline{\phi\phi}. \tag{18}$$

The diffusion of $\overline{u_i \phi}$ is also modelled using the model described by Rodi (1982). This model is given as:

$$\mathscr{D}_{i\phi} = \left[C_\phi \frac{k}{\epsilon}\left(\overline{u_k u_l} \ (\overline{u_i \phi})_{,l} + \overline{u_i u_l} \ (\overline{u_k \phi})_{,l}\right)\right]_{,k}. \tag{19}$$

The dissipation of $\overline{u_i \phi}$ is neglected on the basis of the high turbulent Reynolds number assumption.

The model coefficients appearing in the scalar-flux equation are summarized as:

$$\{C_\phi, C_{1\phi}, C_{2\phi}, C_{3\phi}\} = \{0.15, 2.90, 0.40, 0.40\}. \tag{20}$$

2.4. Scalar intensity transport equation

The scalar intensity, $\overline{\phi\phi}$, which appears in the scalar-flux transport equation, is an additional second-moment correlation which must be solved for in a second-moment stress/flux closure. The transport equation for $\overline{\phi\phi}$ is given as:

$$\frac{\partial \rho \overline{\phi\phi}}{\partial t} + (\rho \overline{U}_k \ \overline{\phi\phi})_{,k} = \rho(\mathscr{D}_{\phi\phi} + \mathscr{P}_{\phi\phi} - 2\epsilon_{\phi\phi}). \tag{21}$$

The terms in parenthesis on the right-hand side represent the diffusion, production and dissipation respectively of $\overline{\phi\phi}$. Models for each process were obtained from Rodi (1982) and are given as:

$$\mathscr{D}_{\phi\phi} = \left[\left(\rho C_{\phi\phi}\frac{k}{\epsilon}\overline{u_k u_l} + \Gamma^\phi\right)\overline{\phi\phi}_{,l}\right]_{,k}, \tag{22}$$

$$\mathscr{P}_{\phi\phi} = -2\rho\overline{u_k\phi}\ \overline{\Phi}_{,k}, \tag{23}$$

$$\epsilon_{\phi\phi} = -\frac{\rho}{R}\frac{\epsilon}{k}\overline{\phi\phi}. \tag{24}$$

The model coefficients for the scalar intensity equation are:

$$\{C_{\phi\phi}, R\} = \{0.10, 0.50\}. \tag{25}$$

2.5. Transport of ϵ equation

The isotropic dissipation rate, ϵ, appears in many of the model relations used in the Reynolds-stress, scalar-flux and scalar intensity equations. ϵ is obtained from the following modelled transport equation (Launder, 1989):

$$\frac{\partial\rho\epsilon}{\partial t} + (\rho\overline{U}_k\ \epsilon)_{,k} = \left[\rho C_\epsilon \frac{k}{\epsilon}(\overline{u_k u_l}\epsilon_{,l})\right]_{,k} + \frac{1}{2}\rho C_{\epsilon 1}\frac{\epsilon}{k}\mathscr{P}_{kk} + \frac{1}{2}\rho C_{\epsilon 3}\frac{\epsilon}{k}\mathscr{G}_{kk} - \rho C_{\epsilon 2}\frac{\epsilon^2}{k}, \tag{26}$$

where the model coefficients are given as:

$$\{C_\epsilon, C_{\epsilon 1}, C_{\epsilon 2}, C\epsilon 3\} = \{0.14, 1.44, 1.92, 0.80\}. \tag{27}$$

2.6. Additional modelling consideration

It was pointed out in Section 1 that turbulence in the vicinity of the interface is acutely attenuated to the extent that the interface appears as a barrier between the active and non-active layers. Thus, an additional modelling consideration in the Reynolds-stress and scalar-flux transport equations for sharply stratified flows is the attenuation of turbulence *at-a-distance* in the region near the interface. An experimental study by Hannoun et al. (1988) found that the attenuation of turbulence and the effects of the anisotropy created by a sharp interface are confined to the large turbulence scales and are similar to the effects created by a solid wall. On this basis, we approximate the inhibiting effect of the interface in the present study by implementing standard wall-reflection models in the $\overline{u_i u_j}$ and $\overline{u_i\phi}$ equations. These wall-reflection models are implemented as extensions to Eqs. (5) and (15), respectively and are given as:

$$\pi_{ij,w} = \left[C_1'\frac{\epsilon}{k}\left(\overline{u_n u_n}\ \delta_{ij} - \frac{3}{2}\overline{u_n u_i}\ \delta_{nj} - \frac{3}{2}\overline{u_n u_j}\ \delta_{ni}\right) + C_2'\left(\pi_{nn,2}\ \delta_{ij} - \frac{3}{2}\pi_{ni,2}\ \delta_{nj} - \frac{3}{2}\pi_{nj,2}\ \delta_{ni}\right)\right]\cdot f, \tag{28}$$

$$\pi_{i\phi,w} = \left[C_{\phi 1}'\ \frac{\epsilon}{k}\ \overline{u_k\phi}\ n_k n_i\right]\cdot f, \tag{29}$$

where $\{C_1', C_2', C_{\phi 1}'\} = \{0.50, 0.30, 0.25\}$. These models were developed on the basis of the observed effect of solid boundaries on turbulence in simple shear flows and, as such, are empirical-based models. The function f is defined as $f = (l/x_n)$, where l is the local length scale of the turbulence defined by $l = \kappa k^{3/2}/\epsilon C_\mu$, and x_n is the normal distance to the sharp interface. The additional coefficients are given as $\{C_\mu, \kappa\} = \{0.09, 0.41\}$. Using these models, turbulence is most strongly attenuated when the local length scale is greater than the distance to the interface, but the models do attenuate turbulence at all distances.

3. Discretization of mean transport equations

The discretization of the governing field equations and the present numerical method are now outlined for the one–dimensional domain shown in Fig. 1. Since the non-active layer has essentially no influence on the entrainment through the interface, it is not necessary to solve for the flow in this region. As such, the computational domain is arranged to cover only the active layer and the interfacial region, with the upper, *je* control-volume situated partly above the interface in the non-active layer. As the computations proceed in time, the movement of the interface is predicted, and the grid adapts to this movement such that the initial *arrangement* of control-volumes is maintained for the entire simulation. Using this arrangement, the *je* node is essentially *pinned* to the interface, and this position serves as the reference for x_n in the wall-reflection models.

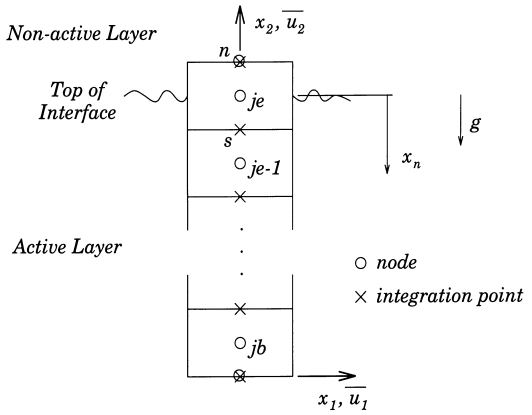

Fig. 1. Computational domain, notation and coordinate system for stably stratified mixing problem.

The transport equations are discretized using the finite-volume formulation of Patankar (1980). Also, the method outlined by, for example, Raithby et al. (1995) was used in the discretization to make the equations applicable on an adaptive grid. Implementation of the adaptive method is described briefly in what follows. We start by integrating the conservation of mass equation,

$$\frac{\partial\rho}{\partial t} + (\rho\ \overline{\mathscr{U}}_i)_{,i} = 0 \tag{30}$$

over a time, Δt and an arbitrary control-volume, $\mathscr{V}$:

$$\int_{\mathscr{V}}\int_{t}^{t+\Delta t}\frac{\partial\rho}{\partial t}\mathrm{d}t\,\mathrm{d}\mathscr{V} + \int_{\mathscr{V}}\int_{t}^{t+\Delta t}\frac{\partial\rho\ \overline{\mathscr{U}}_i}{\partial x_i}\mathrm{d}t\,\mathrm{d}\mathscr{V} = 0. \tag{31}$$

In Eq. (31), $\overline{\mathscr{U}}_i = \overline{U}_i - U_g$ where $\overline{U}_i$ is the fluid velocity (which is zero in the present computations) and U_g is the grid velocity. The transport term is then transformed using Gauss divergence theorem resulting in:

$$\int_{\mathscr{V}}\int_{t}^{t+\Delta t}\frac{\partial\rho}{\partial t}\mathrm{d}t\,\mathrm{d}\mathscr{V} + \int_{\mathscr{S}}\int_{t}^{t+\Delta t}\rho\overline{\mathscr{U}}_i\cdot n_i\,\mathrm{d}t\,\mathrm{d}\mathscr{S} = 0, \tag{32}$$

where $\mathscr{S}$ is a surface and n_i is the unit normal to the surface. Carrying out the integrations and subsequent rearrangement leads to the discrete form of the conservation of mass equation, valid for a moving grid

$$\frac{M_P - M_P^o}{\Delta t} + \dot{m}_n - \dot{m}_s = 0 \tag{33}$$

Next, to obtain the discrete field equations, each of the modelled transport equations must be integrated and rearranged appropriately. As an example, Eq. (1) is first integrated over a time Δt and an arbitrary control–volume $\mathscr{V}$. From this, Eq. (33) multiplied by $\overline{\Phi}_P$ is subtracted and the result is:

$$\frac{M_P^{\circ}\overline{\Phi}_P - M_P^{\circ}\overline{\Phi}_P^{\circ}}{\Delta t} + \frac{(1-\alpha_n)}{2}\left(\overline{\Phi}_N - \overline{\Phi}_P\right)\dot{m}_n - \frac{(1+\alpha_s)}{2}\left(\overline{\Phi}_S - \overline{\Phi}_P\right)\dot{m}_s = D_n\left(\overline{\Phi}_N - \overline{\Phi}_P\right) - D_s\left(\overline{\Phi}_P - \overline{\Phi}_S\right) - M_P\frac{d\overline{u_2\phi}}{\partial x_2}, \quad (34)$$

where $\dot{m}_n$ and $\dot{m}_s$ are the mass fluxes, and D_n and D_s the diffusion coefficients through the north and south faces of the control-volume. The diffusion coefficients are given as, for example, $D_n = (\Gamma^{\Phi}A_n)/(x_{2,N} - x_{2,P})$. The advection terms, on the left-hand side of Eq. (34), were obtained using a simple upwind scheme whereby α (the weighting factor) has a value of either 1 or -1, depending on the direction of $\dot{m}$. This weighting for α was deemed valid on the basis that the mass flux through the control-volume faces is due only to the grid movement (for the present zero-flow case).

Special consideration was required in the discretization of many of the source terms in the discrete transport equations. Foremost was the requirement of a special technique to maintain the coupling between the $\overline{\Phi}$ and $\overline{u_2\phi}$ equations. The technique that was adopted was a fourth-order smoothing similar to that described by Rhie and Chow (1983) for the pressure–velocity coupling. Additionally, consideration was given to the source terms in the $\overline{u_1u_1}, \overline{u_2u_2}, \overline{\phi\phi}$ and ϵ equations to ensure that positive definition was maintained throughout the iterative solution procedure.

3.1. Prediction of interfacial movement

The implicit prediction of the movement of the interface was based on a special solution of the discrete mean scalar equation (Eq. (34)) for the upper-most (*je*) control-volume. As was discussed in Section 1, experimental observations indicate that the interface acts as a barrier between the active and non-active layers, and that the turbulence in the active layer is sharply attenuated at the interface. Thus, for the upper-most control-volume, we assume that $\overline{\Phi}_{je} = \Phi_{\infty}$, and that no turbulence exists at its north face. With these assumptions, the advection and diffusion of $\overline{\Phi}$ through the north face of the *je* control-volume are exactly zero. Furthermore, the time dependent term disappears because the non-active layer is assumed to be temporally constant. The equation for $\overline{\Phi}$ in the *je* control-volume is then simplified to:

$$-\left(\overline{\Phi}_{je-1} - \overline{\Phi}_{je}\right)\dot{m}_s = -D_s\left(\overline{\Phi}_{je} - \overline{\Phi}_{je-1}\right) - M_{je}\left.\frac{d\overline{u_2\phi}}{dx_2}\right|_{je}, \quad (35)$$

where α_s has been assigned a value of 1 so that the advection through the south face is maintained in the balance which predicts the interfacial movement.

Next, the mass flux, $\dot{m}_s$ in Eq. (35), is recast as

$$\dot{m}_s = -\frac{\rho A_s}{\Delta t}\Delta h, \quad (36)$$

where Δh is the movement of the interface over the time-step Δt. Substitution of Eq. (36) and $\overline{\Phi}_{je} = \Phi_{\infty}$ into Eq. (35), and subsequent rearrangement gives:

$$\left[\left(\overline{\Phi}_{je-1} - \Phi_{\infty}\right)\frac{\rho A_s}{\Delta t}\right]\Delta h = D_s\overline{\Phi}_{je-1} - D_s\Phi_{\infty} - M_{je}\left.\frac{d\overline{u_2\phi}}{dx_2}\right|_{je}. \quad (37)$$

In this equation, the movement of the grid, Δh, appears implicitly and is solved in the solution matrix in place of $\overline{\Phi}_{je}$, which is known a priori to be Φ_{∞}. The movement of the interface over time-step Δt is therefore predicted as a compensation for the net transport of $\overline{\Phi}$ (i.e. entrainment) through the south face of *je*, to maintain the level $\overline{\Phi}_{je} = \Phi_{\infty}$ within the control–volume.

Between each iteration of the nonlinear loop, the movement Δh is applied to the *je* node, and also distributed monotonically through the one-dimensional domain below the $je-1$ control-volume to maintain a relatively uniform grid spacing as the depth of the active layer grows (or shrinks). In this manner, each time-step yields a converged value for the interfacial movement, and thus entrainment, in addition to the six other dependent variables $\{\overline{\Phi}, \overline{u_2\phi}, \overline{\phi\phi}, \overline{u_1u_1}, \overline{u_2u_2}, \epsilon\}$.

4. Predictions in oscillating-grid turbulence

To demonstrate the viability of the present method, computations have been carried out for several cases of one-dimensional mixing across a sharp, shear-free interface. In all cases, the fluid system was modelled as water and the sharp, stable interface was modelled using a steep temperature variation. The domain shown in Fig. 1 is representative of the domain used for all of the present computations. The fluid domain was initialized as being uniform at some reference temperature. The steep temperature variation was imposed by assigning the level of $\overline{\Phi}$ at the *je* node to a constant value that was somewhat higher than the initial, constant temperature of the underlying domain.

Boundary conditions were imposed on the upper and lower boundaries. On the upper boundary, the temperature was assigned the same value as $\overline{\Phi}_{je}$ and the remaining quantities $\{\overline{u_2\phi}, \overline{\phi\phi}, \overline{u_1u_1}, \overline{u_2u_2}, \epsilon\}$ were all set to zero. This condition is based on the observed effect of the interface on the turbulence. The lower boundary of the domain was assumed to be just above the oscillating-grid in the fully turbulent region. In this region, the fluid is well mixed and thus, zero gradients were imposed for $\overline{\Phi}$, $\overline{u_2\phi}$ and $\overline{\phi\phi}$. The conditions for the mechanical turbulence field were obtained from Hopfinger and Toly (1976) and are given in Table 1. These values were chosen so that the numerically imposed values would be representative of what could be expected in a laboratory experiment. Table 1 also gives values of the Reynolds numbers based on the integral length scale, l, and the Taylor microscale, λ, to indicate that the high Re_t assumption is justified. Recall that for oscillating-grid turbulence, the Reynolds number is approximately constant for a significant distance from the grid (see Hopfinger and Toly, 1976; Straatman et al., 1998). The values of ϵ in Table 1 were calculated from:

$$\epsilon = \mathscr{A}_{\epsilon}\frac{u_{1o}^3}{l_o}, \quad (38)$$

where $\mathscr{A}_{\epsilon} = 0.61$ and the integral length scale is given by $l_o = 0.25x_2$. The two different sets of conditions that are given in Table 1 represent a low and a high intensity turbulence source, and were both utilized in the present computations.

A grid and time-step independence study was carried out to ensure that the reported results were independent of the grid density and the time-step size. The results of this study are included in Appendix A.

Table 1
Conditions for mechanical turbulence field on lower boundary

Condition	$\overline{u_1u_1}$ [m^2/s^2]	$\overline{u_2u_2}$ [m^2/s^2]	ϵ [m^2/s^3]	Re_l	Re_λ
HT-1	0.00168	0.00242	0.00210	≈ 800	≈ 138
HT-2	0.00436	0.00627	0.00901	≈ 850	≈ 143

4.1. Presentation of results

The quantity of greatest interest in the present study is the rate of entrainment across the sharp interface. To be consistent with previous literature, and to facilitate direct comparisons with experimental data, the entrainment is presented here as a function of the local Richardson number, which is a measure of the local stability. For oscillating-grid turbulence, entrainment laws take the form:

$$u_e/u_{1o} \propto \mathrm{Ri}^{-n}, \tag{39}$$

where u_e is the entrainment velocity obtained from $\Delta h/\Delta t$, u_{1o} the horizontal RMS fluctuating velocity, Ri the local Richardson number, and n an exponent which has been reported in the range $1.0 \leqslant n \leqslant 1.50$. The local Richardson number is defined as:

$$\mathrm{Ri} = g\frac{\Delta\rho}{\rho}\cdot\frac{l_o}{u_{1o}^2}, \tag{40}$$

where $\Delta\rho$ is the difference between the average densities of the active and non-active layers, ρ the density of the non-active layer, and l_o the horizontal integral length scale. The turbulence parameters, u_{1o} and l_o, are taken at the position of the interface, but are representative of what would exist at that position if no interface were present. Thus, u_{1o} and l_o are evaluated from their respective decay and growth laws which are devised from steady grid-generated turbulence in a homogeneous fluid. These laws take the form (see, for example Hopfinger and Toly, 1976):

$$\begin{aligned} u_{1o} &= B_1 x_2^{-1}, \\ l_o &= B_2 x_2, \end{aligned} \tag{41}$$

where B_1 depends on the intensity of the turbulence source and $B_2 \approx 0.25$ (Hopfinger and Toly, 1976).

Finally, since the Boussinesq assumption was implicitly adopted in the modelled field equations, the same assumption is applied to Ri. For relatively small temperature differences, the local Richardson number is modified, using the Boussinesq assumption, to:

$$\mathrm{Ri} \approx g\beta(\Phi_\infty - \overline{\Phi})\frac{l_o}{u_{1o}^2}. \tag{42}$$

4.2. Predictions of entrainment

The entrainment across the sharp interface dictates the growth of the active layer and thus, the spread or dispersion of stable mixing layers. Computational predictions of entrainment were made for several different cases of one-dimensional mixing across a sharp stable interface due to grid-generated turbulence. The parameters which were altered between cases were the intensity of the turbulence source (as given in Table 1), the initial temperature difference, $\Delta\overline{\Phi}_o$, and the initial depth of the active layer, D_a. Table 2 gives a summary of all of the cases that were computed, and their associated parameters.

Fig. 2 shows the results of Cases 1–7 on logarithmic plots of E versus Ri. Included in Fig. 2 is an envelope which represents the range of some experimentally proposed entrainment laws. The envelope is derived from entrainment laws proposed by McDougall (1979), E and Hopfinger (1986) and Nokes (1988). The results in Fig. 2 indicate that changing the various parameters has a strong influence on the relative start position of the entrainment curves, but relatively less of an effect on the slope and the $E(\mathrm{Ri})$ dependence. Varying the initial depth of the active layer has virtually no effect on the $E(\mathrm{Ri})$ dependence. Varying the source intensity and the sharpness of the interface

Table 2
Summary of computed cases for mixing across a sharp interface due to oscillating-grid turbulence

Name	Source	$\Delta\overline{\Phi}_o$ [°C]	D_a [m]	No. of control-volumes
Case 1	HT-1	10	0.10	160
Case 2	HT-1	15	0.10	160
Case 3	HT-1	20	0.10	160
Case 4	HT-1	10	0.15	160
Case 5	HT-1	10	0.20	160
Case 6	HT-2	10	0.15	160
Case 7	HT-2	20	0.15	160
Case 8	HT-1	10	0.10	320
Case 9	HT-2	10	0.15	320

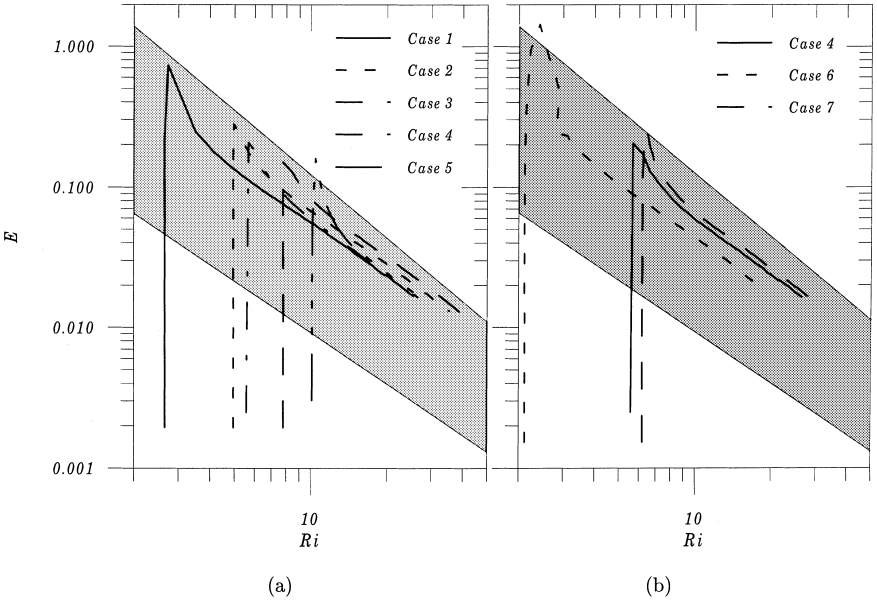

Fig. 2. Entrainment rate E across the interface plotted logarithmically as a function of the local Richardson number Ri.

does have an effect, however, the predicted entrainment curves all have essentially the same slope, $n \approx 1.34$, and the computed results are all within the experimental range. It is not clear from experiments whether all the data should collapse to a single entrainment curve independent of the source intensity or the sharpness of the interface. Among the experiments, there is variability between the different parameters and this may partially explain the differences between the proposed entrainment laws. The results that are important to note from the present computations are that all of the predicted entrainment curves follow the same slope, and more importantly, that the curves all lie well within the envelope of experimental measurements.

Fig. 3 shows the results of Cases 8 and 9 along with the detailed experimental data from E and Hopfinger (1986). Both the computational and experimental data span nearly two decades of Ri. The computational predictions represent nearly 4 h of simulated time over which the active layer grows nearly 0.5 m. This is the reason why Cases 8 and 9 utilized 320 control-volumes instead of 160. The computed results lie slightly below a centerline passing through the experimental data, but overall, the predicted results are in excellent agreement with experiments.

To summarize, all of the computational results for entrainment are in excellent agreement with the experimental data of stable mixing due to oscillating-grid turbulence. Since the entrainment predictions are directly linked to the method devised for predicting the position of the interface, the computational method has also been initially validated. Furthermore, the assumptions made in the development of the method are confirmed. The most pervasive assumptions were that the interface acted as a barrier between the active and non-active layers, and that the entrainment process was driven by the turbulence in the active layer. These assumptions led to the discretization of the active layer *only*, the development of the method for predicting the interfacial movement, and the imposition of zero turbulence conditions on the upper boundary.

4.3. Predictions of turbulence structure

While the predictions of entrainment are most important for determining the dispersion of the active layer, it is the underlying turbulence that drives the entrainment process, and thus the structure of the turbulence is also of interest. The turbulence field evolves rapidly at the beginning of each simulation, followed by a very slow continuous evolution as fluid is entrained and the sharp interface *creeps* farther away from the turbulence source. Fig. 4 shows the results for the normalized horizontal and vertical RMS velocities from Case 1. The coordinate ξ on the abscissa represents the distance from the interface and is normalized by the value of l_o at the position of the interface. The velocities used to normalize the RMS horizontal and vertical fluctuating velocities are those given in Eq. (41). By normalizing the RMS velocities in this manner, Fig. 4 shows only the changes that the turbulence undergoes when the layer is sharply stratified. Included in Fig. 4 are experimental data from Hannoun et al. (1988). It is evident from Fig. 4 that the predicted turbulence fields are only in qualitative agreement with the experimental data. The computed results indicate an attenuation of the normal fluctuating velocity $\overline{u_2}$, and a transfer of energy from $\overline{u_2}$ to $\overline{u_1}$ in the vicinity near the interface, in accordance with the experimental data. However, the computed turbulence fields are lower than their homogeneous-fluid values in the entire domain, a trend not observed from the experiments.

The transport of all quantities in the active layer is essentially driven by the vertical fluctuating velocity. According to

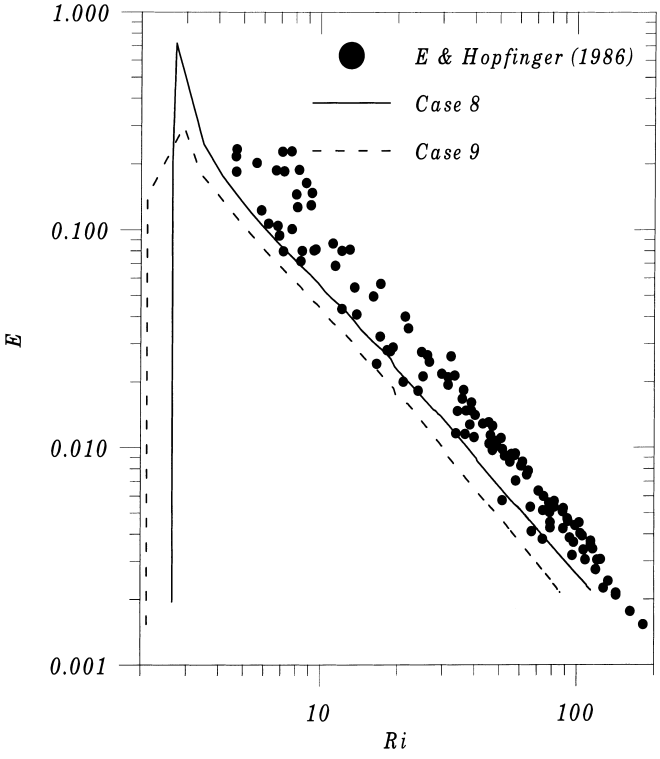

Fig. 3. Entrainment rate E across the interface plotted logarithmically as a function of the local Richardson number Ri.

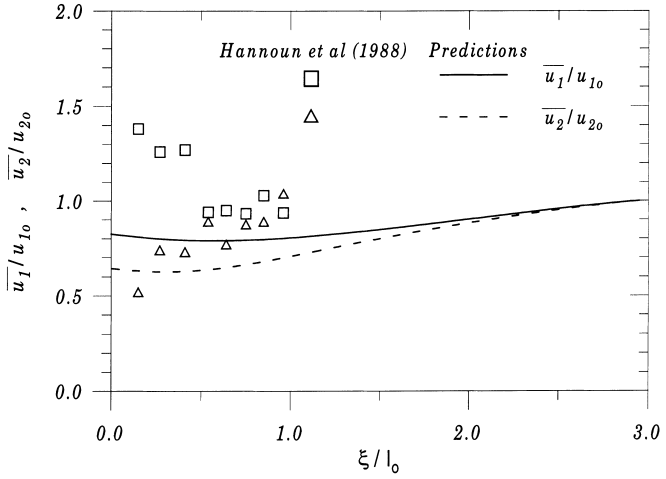

Fig. 4. Variation of non-dimensional normal and planar RMS fluctuating velocities with the non-dimensional distance from the interface, ξ/l_o.

Fig. 4, the predicted vertical fluctuating velocity approaches its measured value near the interface, but the approach is made smoothly over the entire layer. The measured results indicate that changes to the fluctuating velocity fields only occur in the region within one length scale of the interface. Note that the attenuation of the turbulence is partly due to the wall-effect of the interface, and partly due to the stratification in the active layer. In the real case, the wall-effect essentially ceases beyond one integral length scale of the interface because beyond this point the local length scales of the turbulence are less than the distance to the interface. However, the effect of stratification is not restricted by local length scales and can have an influence beyond one integral length scale, depending on the local gradient of $\overline{\Phi}$. In terms of the predicted turbulence fields, it appears that the attenuation due to stratification may be too strong. However, given the limited experimental results for u_{1o} and u_{2o}, it is difficult to assess the predicted values further. The present results of the turbulence structure could potentially be improved by incorporating an alternate formulation to the standard wall-reflection models.

4.4. Predictions of the scalar fields

The scalar-related fields, $\overline{\Phi}$, $\overline{u_2\phi}$ and $\overline{\phi\phi}$, are presented here to complete the physical description of the active layer. Fig. 5 shows the temperature field from Case 8 for three states which correspond to Ri $\approx$ 10, 20 and 30, respectively. In Fig. 5, the vertical coordinate, x_2, has been normalized with the total depth of the layer, D_t, so that $x_2/D_t = 0$ represents the lower boundary and $x_2/D_t = 1.0$ represents the top of the layer. Changes in the temperature field have been normalized with respect to the initial temperature difference, $\Delta\overline{\Phi}_o$. The temperature field at each state is relatively uniform throughout much of the active layer because of the turbulent mixing. As the interface is approached, the temperature field changes sharply towards the level of the non-active layer. Fig. 5 also indicates that as fluid is entrained into the active layer and the local Richardson number increases, the lower portion of the layer becomes more uniform.

The scalar-flux, $\overline{u_2\phi}$, and scalar intensity, $\overline{\phi\phi}$, fields for Case 8 are given in Figs. 6 and 7, respectively, again for three

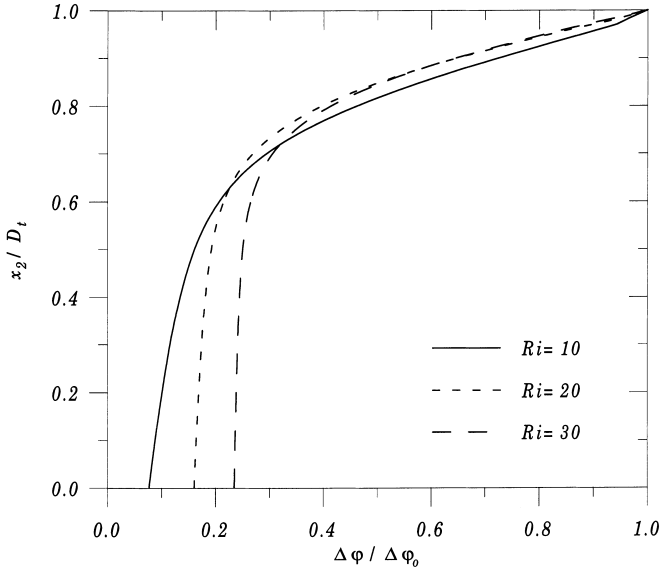

Fig. 5. Variations of normalized temperature field in active layer.

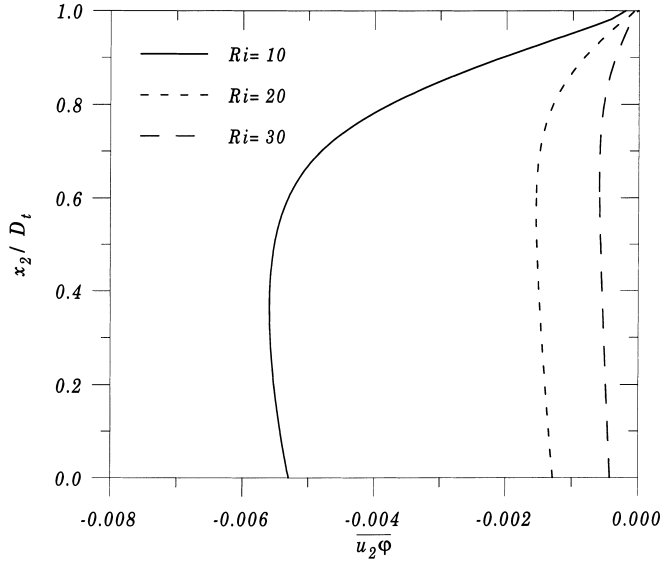

Fig. 6. Variations of scalar-flux, $\overline{u_2\phi}$, in active layer.

states corresponding to Ri $\approx$ 10, 20 and 30. The $\overline{u_2\phi}$ field is negative indicating that energy is transported away from the interface into and throughout the active layer, as expected. Near the interface where the temperature gradient is sharp, the magnitude of $\overline{u_2\phi}$ increases from zero to a terminal value which is essentially maintained throughout the lower portion of the layer. As the Richardson number increases, the the scalar-flux drops significantly because of the reduced entrainment through the interface. However, the shape of the profile is unchanged.

The scalar intensity field reaches a maximum near the interface where the temperature gradient is sharp and then diminishes to nearly zero far away from the interface. As with the scalar-flux, the scalar intensity drops significantly as the Richardson number increases, owing to the decrease in entrainment and thus, transport in the active layer.

5. Conclusions

A computational method for predicting mixing across one-dimensional sharp interfaces has been presented. The method utilizes an adaptive, moving-grid discretization of the governing equations, and solves for the movement of the interface implicitly with the solution of the transport equations. The main advantage of the present method over other numerical methods is that it is only necessary to resolve the active layer to obtain predictions of entrainment at the interface. The predictions of entrainment are in excellent agreement with experimental data. However, predictions of the mechanical turbulence fields are somewhat lower than those measured in experiments. The second-moment turbulence closure performed well in the present computations. With the exception of the diffusion model in the Reynolds-stress equation, standard

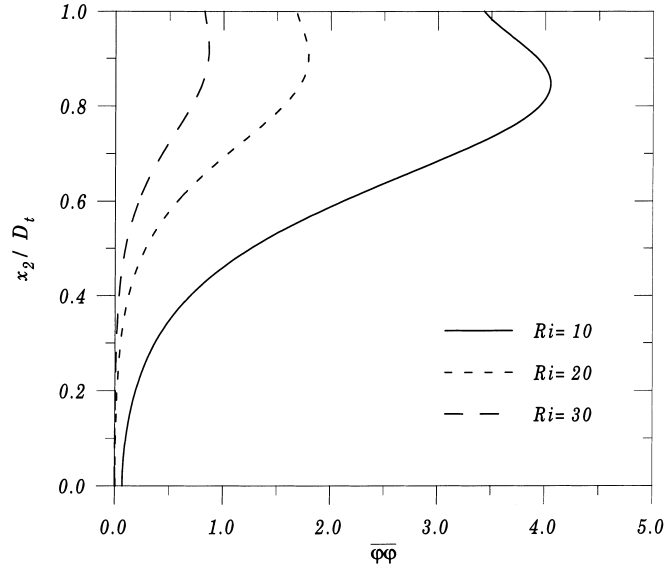

Fig. 7. Variations of scalar intensity, $\overline{\phi\phi}$, in active layer.

relations were used to model the second-moment transport equations. Thus, a near-standard model formulation produced the desired physical effects in a sharply stratified flow.

Finally, the fact that entrainment, and consequently dispersion, can be predicted using this method has important implications in terms of the types of problems one can expect to handle computationally. Focussing computational resources on the active layer alone can result in enormous time savings when solving complex two- and three-dimensional flows. Obviously, much more development is required before such flows can be predicted using this method, but the present predictions provide the first essential benchmark for subsequent development.

The present results effectively demonstrate the viability of the computational method, and the validity of the second–moment turbulence closure in sharply stratified flows.

Acknowledgements

The author gratefully acknowledges the financial support received from the University of Western Ontario, Department of Mechanical and Materials Engineering.

Appendix A. Grid and time-step independence

Both the spatial and time discretization were tested to ensure that the computed results were independent of the grid density and the time-step size. The grid independence study was straightforward, even though the domain, and thus the grid spacing, increased as the computations progressed. Concerning the temporal discretization, it was found that running an entire simulation at the largest possible *initial* time-step was impractical. Since the solution fields for turbulence were initialized to zero, very small time-steps were required to advance the solution through the initial rapid transients. After a short time (about 10–20 s of simulated time), the rapid transients diminished and the time-steps could be increased significantly for the remainder of the computational run. Time-step schemes were set up whereby a small time-step would be used for a short initial period, and then a larger time-step would be used for the remainder. In carrying out the time-step independence study, all of the time-steps in a particular scheme were divided in half.

The case devised for the grid and time-step independence study was to predict the total interfacial movement over 600 s of an initially 0.1 m deep layer with a sharp 10°C change in temperature. The boundary conditions for the turbulence field were taken as HT-1 (see Table 1). Computations were performed using 20, 40, 80, and 160 control-volumes and time-step schemes of 0.05–1.0 s and 0.1–2.0 s (for the 160 control-volume case). The resulting total interfacial movements are given in Table 3.

Table 3 indicates that predictions within 4% can be achieved on very coarse grids, but to obtain predictions that are grid-converged to within 2.5% requires 160 control volumes. The two time-step schemes used give essentially the same predictions, thus the larger time-step scheme was utilized in the remainder of the computations.

Table 3
Results for total interfacial movement for grid and time-step independence study

No. of Control-volumes	Time-step scheme	Total interfacial movement
20	0.1–2.0	0.3876
40	0.1–2.0	0.3742
80	0.1–2.0	0.3608
160	0.1–2.0	0.3520
160	0.05–1.0	0.3517

References

Daly, B.J., Harlow, F.H., 1970. Transport equations in turbulence. Phys. Fluids 13 (11), 2634–2649.

De Silva, I.P.D., Fernando, H.J.S., 1994. Oscillating grids as a source of nearly isotropic turbulence. Phys. Fluids 6, 2455–2464.

De Silva, I.P.D., Fernando, H.J.S., 1996. Some aspects of mixing in a stratified turbulent patch. J. Fluid Mech. 240, 604–625.

Dickinson, S.C., Long, R.R., 1978. Laboratory study of the growth of a turbulent layer of fluid. Phys. Fluids 21, 1698–1701.

Dickinson, S.C., Long, R.R., 1983. Oscillating-grid turbulence including the effect of rotation. J. Fluid Mech. 126, 315–333.

E, X., Hopfinger, E.J., 1986. On mixing across an interface in stably stratified fluid. J. Fluid Mech. 166, 227–244.

Fernando, H.J.S., Long, R.R., 1985. On the nature of the entrainment interface of a two-layer fluid subjected to zero-mean-shear turbulence. J. Fluid Mech. 151, 21–53.

Hannoun, I.A., Fernando, H.J.S., List, E.J., 1988. Turbulence structure near a sharp density interface. J. Fluid Mech. 189, 189–209.

Hopfinger, E.J., Toly, J.A., 1976. Spatially decaying turbulence and its relation to mixing across density interfaces. J. Fluid Mech. 78, 155–175.

Launder, B.E., 1989. Phenomenological modelling: present and future. In: Whither Turbulence? Turbulence at the Crossroads. Springer, Berlin, pp. 439–485.

Lumley, J.L., 1978. Computational Modelling of Turbulent Flow. In: Advances in Applied Mechanics, vol. 18, Academic Press, pp. 123–176.

McDougall, T.J., 1979. Measurements of turbulence in a zero-mean-shear mixed layer. J. Fluid Mech. 94, 409–431.

Nokes, R.I., 1988. On the entrainment rate across a density interface. J. Fluid Mech. 188, 185–204.

Patankar, S.V., 1980. Numerical Heat Transfer and Fluid Flow. Hemisphere, Washington, DC.

Raithby, G.D., Xu, W.X., Stubley, G.D., 1995. Prediction of incompressible free surface flows with an element-based finite volume method. Comput. Fluid Dynamics J. 4 (3), 353–371.

Rhie, C.M., Chow, W.L., 1983. Numerical study of the turbulent flow past an airfoil with trailing edge separation. AIAA J. 2, 1527–1532.

Rodi, W., 1982. Turbulent Buoyant Jets and Plumes. Pergamon Press, Oxford.

Straatman, A.G., Stubley, G.D., Raithby, G.D., 1998. An examination of diffusion modelling in second-moment closures using zero-mean-shear turbulence. AIAA J. 36 (6), 929–935.

Thompson, S.M., Turner, J.S., 1975. Mixing across an interface due to turbulence generated by an oscillating grid. J. Fluid Mech. 67, 349–368.